Adaptive Control of Power Electronic Drives for Servomechanical Systems

Deron K. Jackson, *Member, IEEE*, Steven B. Leeb, *Member, IEEE*, and Steven R. Shaw

***Abstract*—This paper presents adaptive-control schemes that estimate load-model parameters and adaptively "tune" a digital controller for an inductively-coupled power delivery circuit. Estimation algorithms are presented that utilize specific recursive formulations, which provide adequate noise immunity in a power-electronic environment. The techniques are demonstrated using a servomechanical system and a 1.5-kW prototype power electronic drive.**

***Index Terms*—Adaptive control, inductive coupling, power electronics.**

I. Introduction

IN CONTRAST to controllers for typical regulation applications, servomechanical systems generally require a controller whose transient performance is verifiably guaranteed over a wide range of operating conditions. Also, for adequate tracking performance, the controller may need to respond relatively swiftly to command changes or load disturbances. An array of servomechanical control problems exist where slow variations (compared to control bandwidth) in mechanical properties, loading, or external disturbances lead to changes in the load model parameters. Such changes can adversely affect even relatively robust control designs.

Adaptive or "self-tuning" controls adjust automatically in response to system changes. Adaptive control systems have been widely studied [1], [2], and generally are two step processes of system parameter estimation and control adaptation. Both tasks must be accomplished on-line to permit the controller to track time-varying system parameters. This imposes certain limits on implementations. In addition, the adaptation algorithm must be suitable for digital implementation and sufficiently robust to noise. This paper addresses these concerns and presents techniques specifically suited to power electronic and digital control environments.

II. System Overview

A number of circuit topologies for inductively coupled power transfer in servomechanical applications are reviewed in [3]. One power electronic drive, for example, is a unidirectional power transfer coupling that draws power from the ac utility through a high power factor pre-regulator. Power is transferred to the load through a half-bridge inverter that energizes a separable transformer or inductive coupling. Another drive explored in [3] employs a high power factor pre-regulator capable of bidirectional power transfer, to or from the electric utility, and either a full-bridge or symmetric half-bridge inverter circuit capable of transferring power to or from a load through the inductive coupling.

An inductive coupling provides features including: safety isolation; a separable or sliding, nonohmic electro-mechanical interface; and, often, the possibility of transferring power across an unbroken environmental interface, e.g., the skin of a patient receiving an externally powered *in-vivo* implant, or a wall in a transportation system. The advantages and engineering challenges of operating this type of coupling and the associated drive circuitry over a range of power levels and applications have been reviewed in numerous publications, including [4]–[9], among others.

In [10]–[12], we exploited large-signal linear models for developing controllers for the inductively-coupled power electronic drives used in [3]. Large-signal linear models are essential for developing controllers with verifiable performance in tracking applications. The general multirate digital control techniques developed in [3], [11], and [12], and presume that the driving-point impedance or other input-to-output behavior of the load can be described by a linear, time-invariant transfer-function model. The time invariance constraint implies that the differential equations or transfer function describing the load model contains constant coefficients. These coefficients must be known in order to apply conventional design techniques. Not surprisingly, a number of applications do not fit this description.

The next sections present techniques for estimating the slowly varying coefficients of a load model for a load driven by an inductively coupled power electronic drive. These techniques can be used to update the gains of a controller to ensure specified performance under load changes. The parameter estimation and adaptive controller demonstrations are constructed using a prototype 1.5 kW inductively coupled drive (described in detail in [3]). However, the estimation techniques could be used in virtually any on-line, digitally controlled power electronic application. Also, since many power electronic drives employ a fixed (nonseparable) transformer for isolation or voltage conversion, the demonstration of these control techniques with an inductively coupled (separable transformer) drive, which is very similar to a fixed transformer drive, does not limit their applicability.

Manuscript received June 18, 1999; revised February 24, 2000. This work was supported by AMP, Incorporated, the National Science Foundation through a CAREER award, an MRSEC grant to the Center for Materials Science and Engineering, the Massachusetts Institute of Technology, Intel, and Hewlett-Packard.

D. K. Jackson is with Adept Technology, San Jose, CA 95192 USA.

S. B. Leeb is with the Laboratory for Electromagnetic and Electronic Systems and the Center for Materials Science and Engineering, Massachusetts Institute of Technology, Cambridge, MA 02139 USA.

S. R. Shaw is with Montana State University, Bozeman, MT 59715 USA.

Publisher Item Identifier S 0885-8993(00)09804-5.

III. Parameter Estimation for Power Electronic Devices

A conventional linear estimation problem begins with the assumption that a column vector $\mathbf{y}$ composed of scalar measurements $y[k]$ can be related to the product of a "regressor" matrix $\mathbf{R}$ (composed of row vectors $\mathbf{r}[k]^T$) and a column vector of parameters $\boldsymbol{\theta}$ which characterize the system [2]

$$\mathbf{R}\boldsymbol{\theta} = \mathbf{y}. \tag{1}$$

In a typical application, a large number (relative to the number of parameters in $\boldsymbol{\theta}$) of measurements are made to assemble the $\mathbf{y}$ vector. The system is overconstrained. Generally, no vector $\boldsymbol{\theta}$ can be found that precisely satisfies (1). The least-squared error solution

$$\hat{\boldsymbol{\theta}} = \left(\mathbf{R}^T\mathbf{R}\right)^{-1}\mathbf{R}^{\mathbf{T}}\mathbf{y} \tag{2}$$

minimizes the sum of the squared errors, i.e., the 2-norm of the vector $\mathbf{y} - \mathbf{R}\hat{\boldsymbol{\theta}}$. (The "hat" notation is used throughout this paper to indicate estimated quantities.) The critical choice of model parameterization determines $\mathbf{R}$. The presence of disturbances in $\mathbf{R}$ or correlation between the columns of $\mathbf{R}$ and disturbances in $\mathbf{y}$ will result in biased parameter estimates. Also, the numerical condition of $\mathbf{R}$, which depends on the richness of available measurements, determines the practical ease with which (2) may be solved. Generally, direct numerical solution of (2) is not the best approach for finding $\hat{\boldsymbol{\theta}}$, and recursive formulations based on this equation may also be numerically inferior to more clever solution techniques. However, given sufficiently rich measurements, all of these estimation approaches are generally functional for application with thriftily modeled servomechanical drives.

A. Recursive Least-Squares Estimation

Recursive least-squares (RLS) estimation is an iterative reformulation of the conventional least-squares solution. Rather than waiting to accumulate a collection of measurements before estimating the parameter vector, as in conventional least-squares estimation, the estimate $\hat{\boldsymbol{\theta}}$ can be updated as each new measurement is made. The RLS estimator is very attractive for real-time applications. Because the RLS algorithm is recursive, very few data points need to be stored between iterations, and computations occur at specified intervals with a predictable computational complexity.

The recursive least-squares algorithm is shown in (3) below

$$\begin{aligned}
\epsilon[k] &= y[k] - \mathbf{r}[k]^T\hat{\boldsymbol{\theta}}[k-1] \\
\mathbf{g}[k] &= \frac{\mathbf{P}[k-1]\mathbf{r}[k]}{\rho + \mathbf{r}[k]^T\mathbf{P}[k-1]\mathbf{r}[k]} \\
\hat{\boldsymbol{\theta}}[k] &= \hat{\boldsymbol{\theta}}[k-1] + \mathbf{g}[k]\epsilon[k] \\
\mathbf{P}[k] &= \frac{1}{\rho}\left(\mathbf{P}[k-1] - \mathbf{g}[k]\mathbf{r}[k]^T\mathbf{P}[k-1]\right)
\end{aligned} \tag{3}$$

where

$\epsilon[k]$ scalar prediction error;
$\mathbf{g}[k]$ gain vector;
$\mathbf{P}[k]$ weighting matrix [1].

The algorithm in (3) is executed from top to bottom at each iteration of the index k.

For now, assume that the "forgetting factor," ρ, is unity. In this case, after N iterations, the recursive algorithm can, with infinite precision arithmetic, return the exact parameter estimates that would occur using nonrecursive least squares on the same N data points. However, a perfect match requires very specific initial conditions for $\mathbf{P}[k]$. In practice, the matrix $\mathbf{P}[0]$ and the initial parameter vector may be determined by producing initial estimates, perhaps off-line, using conventional least squares. Alternatively, the algorithm could be started with an initial guess at the parameters and a $\mathbf{P}[0]$ matrix set to a large constant multiplied by an identity matrix. Although this can cause large initial transients in the parameter estimate, the large $\mathbf{P}[0]$ helps assure relatively rapid parameter convergence.

The RLS algorithm just described refines its parameter estimates at each iteration. So after N iterations the accuracy of the estimate accumulates the contributions from all $N-1$ previous iterations. This prevents the algorithm from accurately tracking time-varying parameters unless the effect of distant data points can somehow be mitigated. This can be accomplished by setting the forgetting factor ρ to a value less than unity. The forgetting factor modifies the minimization criteria of the RLS algorithm so that errors that occurred at time index $k-i$ are weighted by ρ^i. The number of samples effectively kept in "memory" is roughly proportional to $1/(1-\rho)$ [2].

Exponential forgetting must be tuned with some care for optimum performance. If ρ is chosen too large, it will lead to slow convergence of the estimates, and if chosen too small, it will result in noisy estimates, which are based on too few data points. Thus, the choice of ρ represents a trade-off between parameter tracking and disturbance rejection. Another problem, known as "covariance matrix explosion," may occur during moments of low excitation [2]. In the absence of a significantly exciting input, the quantity $\mathbf{P}[k-1]\mathbf{r}[k]$ will approach zero, in which case $\mathbf{P}[k]$ will begin to increase exponentially. In turn, the parameter estimates become increasingly sensitive to the prediction error $\epsilon[k]$, and the slightest noise or model inaccuracy can lead to erratic or erroneous parameter estimates. In practice, we could attempt to mitigate this effect by skipping the RLS update if a defined variable, such as the output, changes by less than an amount δ between samples.

Recursive estimation is a rich topic that has received much research attention. Many modifications have been proposed to optimize the performance of the basic recursive estimator for noise environments with specific, known probabilistic distributions. Also, note that the performance analyses of the basic least squares approach typically assume that noise or measurement error is confined to the vector of observations and assumes an understood form. In fact, in servomechanical applications of interest, noise often affects both the measurement vector **and** the regressor matrix. Other techniques, e.g., "total" least squares [13], have been developed to provide solutions that are optimal in some sense for these cases. Generally, careful characterization of the noise environment in a power electronic servomechanism, where disturbances may be closely correlated and impulsive or non-Gaussian in nature, is difficult. Experiments with the prototype hardware show that using the RLS estimation technique to determine the parameters of a "state-variable-filtered" plant model can lead to relatively noise-immune parameter es-

timation techniques suitable for the power electronic environment.

B. State Variable Filtering

The term "lambda method" (LM) is used here to describe a modification to the conventional recursive least-squares (RLS) algorithm, which will be referred to as LM-RLS. The technique relies on an "operator transformation" that allows the differentiation operator in a continuous-time (CT) transfer function model to be replaced, in principle, without approximation. The result is a discrete-time (DT) estimation algorithm, which operates on transformed or filtered observations of the input and output data. An estimation algorithm can then be designed around the transformed model. This technique is described briefly in [2] and in other literature under the heading "model transformation" or "state-variable filter," but appears to have been largely overlooked in the power-electronics literature. However, our experiments demonstrate that a substantial reduction in noise sensitivity can be achieved in comparison to conventional RLS.

The LM-RLS technique is developed around a CT transfer function model of the system, e.g., the rational CT transfer function

$$H(s) = \frac{b_1 s^{m-1} + \cdots + b_m}{s^m + a_1 s^{m-1} + \cdots + a_m} \tag{4}$$

where the denominator polynomial has order m and the coefficients a_i and b_i may be time varying. This system function might model the driving point admittance of a battery to be charged, or the through transfer function of a speed-control servomechanism, or, generally, the system function of any plant to be driven and controlled by a power electronic drive. The coefficients of $H(s)$ equivalently describe a linear differential equation model of the system written as

$$\begin{aligned} p^m y(t) + a_1 p^{m-1} y(t) + \cdots + a_m y(t) \\ = b_1 p^{m-1} u(t) + \cdots + b_m u(t) \end{aligned} \tag{5}$$

where p represents the derivative operator (d/dt) and $u(t)$ and $y(t)$ represent the input and output variables of the system with system function (4). An operator transformation can be applied to (5), whereby the p operator is replaced by the causal, low-pass "lambda" operator

$$\lambda = \frac{1}{\tau_\lambda p + 1} \tag{6}$$

where τ_λ is a positive time constant. Using (6) to eliminate p from (5) yields a new linear model, which can be written as

$$\begin{aligned} y(t) + \alpha_1 \lambda y(t) + \cdots + \alpha_m \lambda^m y(t) \\ = \beta_1 \lambda u(t) + \cdots + \beta_m \lambda^m u(t) \end{aligned} \tag{7}$$

where the reformulated parameters α_i and β_i are algebraically related to the starting parameters a_i, b_i, and the time constant τ_λ. In (7) the addends $\lambda y(t)$, $\lambda u(t)$, etc., represent inputs and outputs operated on by λ. The λ operator is a first-order low-pass filter with a time constant τ_λ; "powers" of λ are multiple applications of the operator.

The reformulated parameters from (7) can be estimated directly using the RLS algorithm. Assuming that the filtered CT quantities are available, they can be sampled every T_k s, in synchrony with the corresponding DT algorithm iterated by the index k. At each time step k, the sampled data is compiled into a regressor vector

$$\mathbf{r}[k] = \begin{bmatrix} -\lambda y(kT_k) \\ \vdots \\ -\lambda^m y(kT_k) \\ \lambda u(kT_k) \\ \vdots \\ \lambda^m u(kT_k) \end{bmatrix}$$

and a vector of transformed parameters is computed by the RLS algorithm

$$\hat{\boldsymbol{\theta}}_\lambda[k]^T = \left[\hat{\alpha}_1 \cdots \hat{\alpha}_m \hat{\beta}_1 \cdots \hat{\beta}_m\right].$$

The final operation at each time step is to recover estimates of the starting parameters, $\hat{a}_i$ and $\hat{b}_i$, from their known relationships to $\hat{\alpha}_i$, $\hat{\beta}_i$, and τ_λ.

The convergence properties of the LM-RLS method are strongly affected by the selection of the filter time constant τ_λ. Experimental evidence suggests that τ_λ should not exceed the nominal settling time of the target system. Doing so will unnecessarily slow the convergence rate of the parameter estimates. A compromise may be necessary, however, if τ_λ is increased to attenuate noise from an external source. Conversely, decreasing τ_λ can speed up the convergence rate, but the convergence transient can be expected to become increasingly violent [2]. Nevertheless, the convergence properties of the LM-RLS method demonstrate a marked improvement over the direct RLS approach. This will be demonstrated by the experimental tests in the following sections.

IV. Experiment: Bath Temperature Control

A range of servomechanical control demonstrations were designed, constructed, and documented in [3], including an electric vehicle battery charger, a solvent bath temperature control system, and a motor-speed control system. The temperature control system, described in this section, involved an adaptive controller for a liquid-bath temperature control system. The liquid bath plant benefits from the inherent safety isolation provided by inductive coupling. It is representative of a number of real-world manufacturing and medical applications, which could take advantage of inductive-coupling as a noncontact means to transfer power across an environmental boundary. Because the plant is essentially first order, as will be discussed, the parameters of the plant model can estimated successfully by directly applying the RLS algorithm, without state variable filtering. In the following section, a more complicated example of a motor speed controller will be examined, in which the LM-RLS method is essential for successful real-time on-line estimation.

The experimental setup for the bath system is illustrated in Fig. 1. A 1-kW immersion heater was placed inside a two gallon water bucket. Electrical power for this heater was supplied via

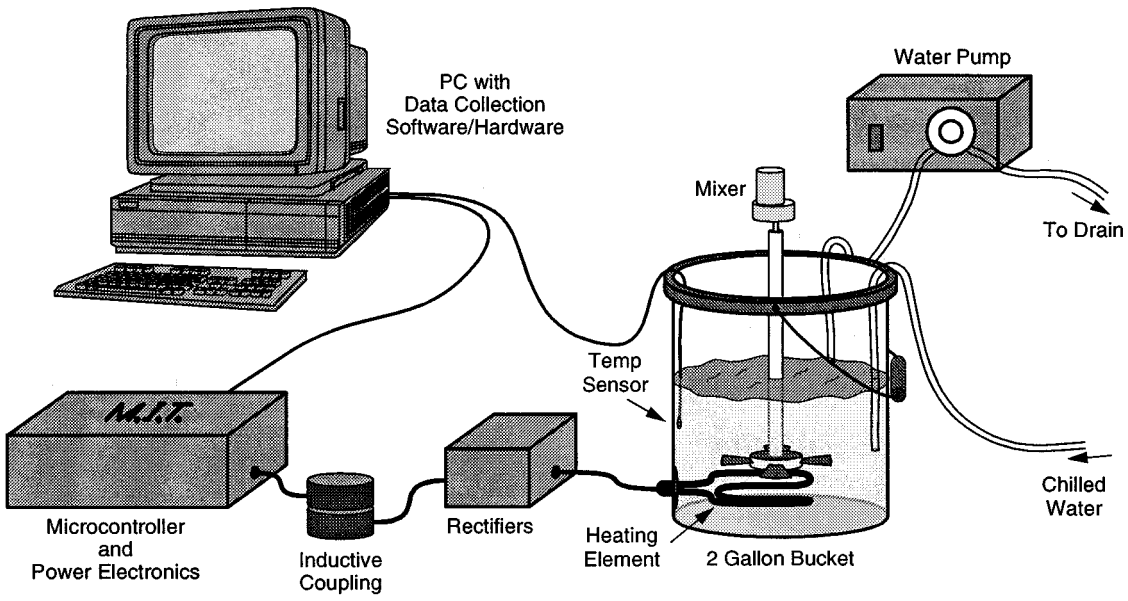

Fig. 1. Setup for bath temperature control experiments.

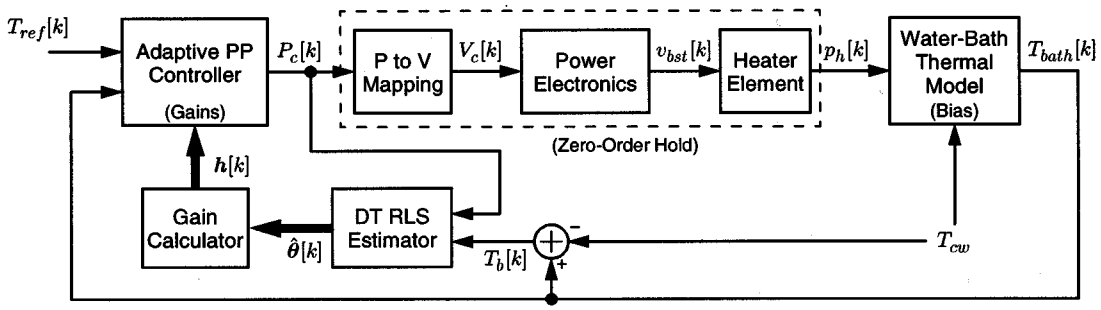

Fig. 2. Block diagram for temperature control experiments.

an inductive coupling and the 1.5-kW prototype power electronic drive. Chilled water was supplied to the bucket at a constant rate from a cold water supply, and excess water was actively pumped out through a drain hose. Adjusting the level of the drain up or down allowed for external control of the water volume, with a range from approximately 0.6–1.5 gallons. A mixer kept the water in constant circulation so that the temperature throughout the bucket was homogeneous.

The personal computer (PC) illustrated in Fig. 1 was used to record experimental data for later analysis. This system recorded two electrical signals: the controlled boost voltage $v_{bst}(t)$ from the output of the pre-regulator in the 1.5 kW inductively-coupled prototype electronic drive, and also the bath temperature $T_b(t)$. For use in control, the bath temperature was also relayed to an embedded 80C196KC digital microcontroller board used to control the power electronics as described in [11] and [3]. It is important to emphasize that the PC in this experimental setup simply and *only* provided archival data collection for later, off-line comparison to experimental results. *All digital control and estimation algorithms were implemented on-board the embedded 80C196KC microcontroller board.* A control panel attached to the microcontroller board provided a user interface for setting control options, temperature setpoints, etc.

A. Control Design

The multi-loop adaptive temperature control system is illustrated in Fig. 2. The system actually consists of three nested control loops. An innermost analog loop (not shown explicitly) controls the waveshaping provided by a unity power factor, interleaved boost pre-regulator in the power electronics block. Next, a digital loop (again hidden in the dashed box), based on a large signal linear model of the boost converter, controls the output voltage of the converter to track with command inputs $V_c[k]$. The output voltage of the boost converter serves as the input to a high-frequency, dc–dc, zero-voltage switched bridge converter that transfers power across a separable inductive coupling to the electrothermal load, represented overall by the dashed box in the figure. The final feedback loop, the adaptive, pole placement (PP) compensated feedback loop, regulates bath temperature by controlling thermal power dissipated in the bath. This DT loops runs at a slower time scale than the inner voltage regulation loop. That is, many time steps of the voltage loop occur in one time step of the thermal loop. The remaining blocks in Fig. 2 represent the adaptive temperature controller. Parameter estimation for this controller was performed using the LM-RLS algorithm.

Fig. 3 shows equivalent load models for the heater and water-bath systems. The circuit on the left models the dc/dc

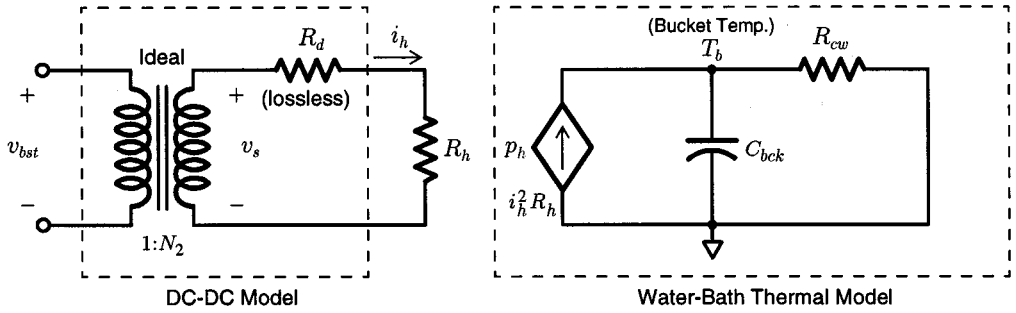

Fig. 3. Equivalent electrothermal load model.

converter with a resistive immersion heater attached. The dc/dc stage energizing the inductive coupling can be modeled as an ideal transformer and a series impedance R_d (representing the droop characteristic of the open loop dc/dc stage). The model also includes a heater resistance R_h. The power dissipated in the heating element is

$$p_h = i_h^2 R_h = \frac{N_2^2 v_{bst}^2 R_h}{(R_d + R_h)^2} \tag{8}$$

where N_2 is the effective turns ratio of the inductive coupling. Equation (8) can be inverted so that the appropriate voltage reference V_c can be found to achieve a target power dissipation P_c. That relationship is

$$V_c = \frac{R_d + R_h}{N_2} \sqrt{\frac{P_c}{R_h}}. \tag{9}$$

Equation (9) is used in the "P-to-V mapping" block of Fig. 2.

The thermal circuit in Fig. 3 models the relationship between p_h, the power dissipated in the heater, and the differential water-bath temperature T_b, measured with respect to the cooling water supply temperature T_{cw}. That is, the cooling water temperature is taken to be the ground or datum reference in the thermal circuit analog shown in Fig. 3. The capacitance C_{bck} in the model represents the heat capacity of the water. The lumped element model of the thermal capacitance of the bath is reasonable because the bath is well mixed. The effective thermal resistance between the bucket temperature and the cooling water temperature is modeled by R_{cw}. Applying Kirchhoff's current law to this thermal equivalent circuit yields the following first-order differential equation:

$$p_h(t) - \frac{T_b(t)}{R_{cw}} = C_{bck} \frac{dT_b(t)}{dt}. \tag{10}$$

From (10), a transfer function relating the Laplace transforms of $p_h(t)$ and $T_b(t)$ can be written

$$H(s) = \frac{T_b(s)}{P_h(s)} = \frac{R_{cw}}{R_{cw} C_{bck} s + 1}. \tag{11}$$

The inner DT voltage loop controlling the output voltage of the boost converter is designed to work quickly on the time scale of the outer DT temperature control loop. This means, for example, that, in combination with the P-to-V mapping, the inner voltage loop might be configured and modeled as a "power-level" zero-order hold (ZOH) on the time scale of the outer thermal loop. This configuration is enabled by the guaranteed dynamics of the large-signal linear voltage loop controller with load power feedfoward discussed in [11] and [3]. Other configurations and modeling possibilities are also discussed in these references, and will be exploited in the next section.

To complete the DT compensator design and determine the closed-loop system behavior, it is necessary to determine the transfer function $\tilde{H}(z)$ for the dashed box in Fig. 2 that relates the z-transform of output temperature to the z-transform of the input voltage command from the PP temperature compensator. With the ZOH configuration, $\tilde{H}(z)$ can be found by applying a step-invariant CT-to-DT transformation [14] to the transfer function $H(s)$

$$\tilde{H}(z) = \frac{b_1}{z + a_1} \tag{12}$$

where

$$b_1 = R_{cw}(1 + a_1) \quad a_1 = -e^{-(T_k / R_{cw} C_{bck})}. \tag{13}$$

The DT transfer function (12) relates z-transforms of the commanded power $P_c[k]$ and the sampled temperature $T_b[k]$. The DT load model in (12) can now be used to design a DT compensator which yields the desired closed-loop performance. The control command $P_c[k]$ for a first-order PP temperature controller is

$$\begin{aligned} P_c[k] = P_c[k-1] &+ h_1 (T_{ref}[k] - T_{bath}[k]) \\ &+ h_2 (T_{ref}[k] - T_{bath}[k-1]) \end{aligned} \tag{14}$$

where $T_{ref}[k]$ is the temperature reference and h_1 and h_2 are feedback gains.

Now, the closed-loop transfer function for the temperature controller is

$$\tilde{H}_{CL}(z) = \frac{(1 + x_1 + x_2) z}{z^2 + x_1 z + x_2} \tag{15}$$

provided the gains h_1 and h_2 are selected according to

$$h_1 = (x_1 - a_1 + 1)/b_1 \quad h_2 = (x_2 + a_1)/b_1. \tag{16}$$

The locations of the closed-loop poles may be located essentially arbitrarily in the z-plane by carefully selecting the control gains h_1 and h_2 to yield the desired denominator in (15).

B. Adaptive Updating

The derivation of this controller assumes that the coefficients of the load model are known. It is possible to estimate these

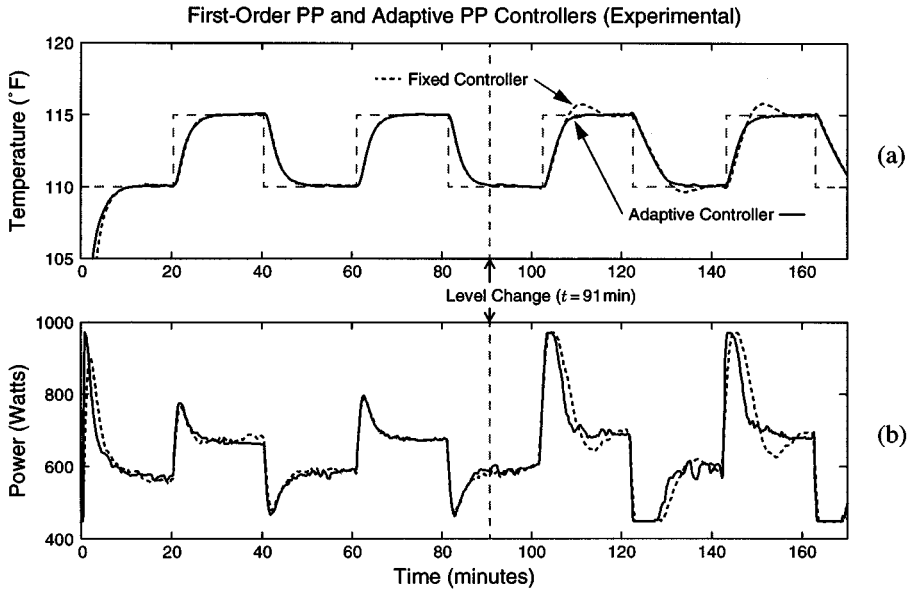

Fig. 4. Results (see text).

coefficients in real-time and use them to adaptively update the controller gains in the event of parameter changes. The adaptive control structure is illustrated in Fig. 2. A discrete-time RLS estimator with exponential forgetting was used to estimate the parameters of DT transfer function (12) on-line. The regressor and parameter estimate vectors for this case are

$$\mathbf{r}[k] = \begin{bmatrix} -T_b[k-1] \\ P_c[k-1] \end{bmatrix} \quad \text{and} \quad \hat{\boldsymbol{\theta}}[k] = \begin{bmatrix} \hat{a}_1 \\ \hat{b}_1 \end{bmatrix}. \tag{17}$$

The RLS algorithm updates the parameter estimates at each step of the index k. The control gains h_1 and h_2 are updated after each iteration in order to achieve a closed-loop transfer function with two real poles at identical locations on the z-axis, e.g., $z_1 = z_2 = m$. Thus, h_1 and h_2 are computed as

$$h_1 = \frac{-2m - \hat{a}_1 + 1}{\hat{b}_1} \quad \text{and} \quad h_2 = \frac{m^2 + \hat{a}_1}{\hat{b}_1}. \tag{18}$$

C. Results

The adaptive temperature control system was implemented in software on the 80C196KC microcontroller board. The C-code source listings can be found in [3]. So that direct performance comparisons could be made, both fixed and adaptive controllers were implemented. The fixed controller was optimized for operation at the low end of the water volume range, approximately 0.6 gallons. The load model parameters for $H(s)$ in (11) were approximated experimentally at this level.

The closed-loop performance of both the fixed and adaptive loops was targeted to have two real poles at $m = 0.80$. A sample period of $T_k = 20$s was used, so the inner- and outer-loop indices are related by $n = Qk$, where $Q = 2400$. The RLS parameter estimation for the adaptive controller was configured with a forgetting factor ρ of 0.99. Thus, approximately 60 min of data is retained in "memory." No initial guess was supplied for the parameters. Rather, the matrix $\mathbf{P}$ was initialized as 10 000 times an identity matrix, and the estimates were allowed to converge on their own. In order to assure stable control during start-up, the fixed controller was engaged for the first 10 min. This allowed time for the estimates to converge before adaptive control was engaged.

Experimental results appear in Fig. 4. In the top graph, labeled (a) in Fig. 4, the response of the fixed and adaptive controllers are shown in comparison to the command reference. The traces in (b) show the power commanded by each controller into the heating element. A square wave in temperature was commanded in order to demonstrate the control performance. In each case, the system began with the fluid level set at 0.6 gal. At this level the closed-loop performance of both the adaptive and fixed temperature controllers is nearly ideal. The step transients are consistent with the closed-loop pole locations, and the tracking performance is good. After approximately 90 min of operation, the fluid level was increased to 1.5 gal. This volume change takes approximately 5 min to occur. The change drives the fixed controller away from its optimal operating point and significant overshoot results. The adaptive controller, on the other hand, quickly adapts to the altered load model, and the desired closed-loop performance is maintained.

Several attempts were made to improve the convergence rate by decreasing the forgetting factor ρ. While it was found that some improvement was possible, the increased noise sensitivity quickly becomes intolerable. As noise susceptibility increases, the accuracy of the parameter estimates degrades, which leads to poor closed-loop performance or even instability. Since parameter tolerance tends to decrease as control complexity increases, higher-order systems offer even less flexibility. For the adaptive speed controller described in the next section, the reformulated LM-RLS estimator proved essential.

V. Experiment: Motor Speed Control

The speed servomechanism described in this section could, for example, model the drive system for an underwater vehicle, where electrical power passes contactlessly through

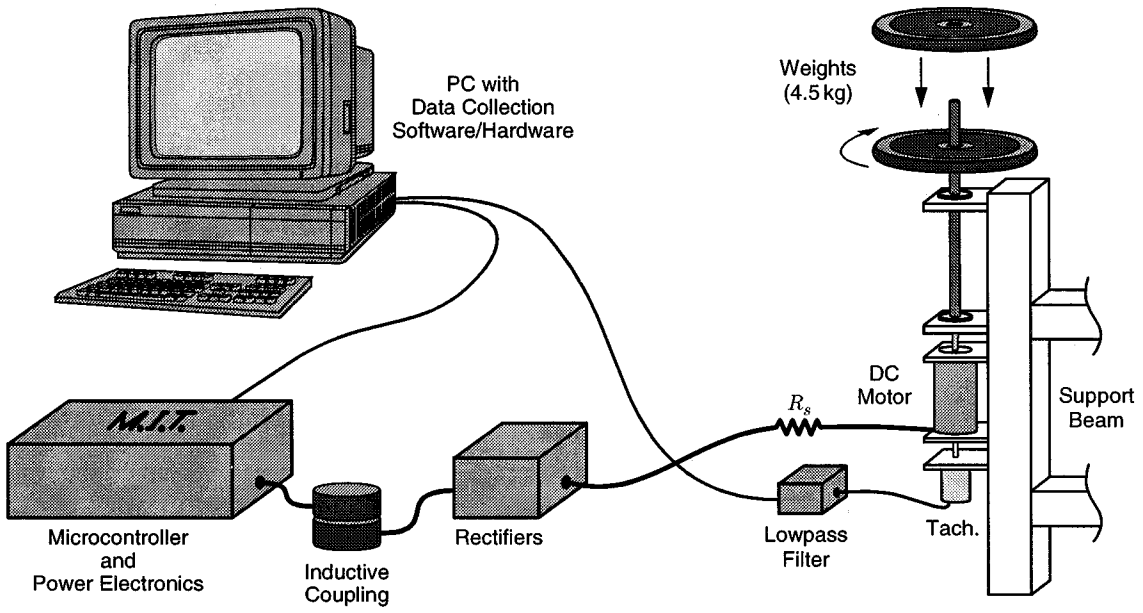

Fig. 5. Setup for motor speed control experiments.

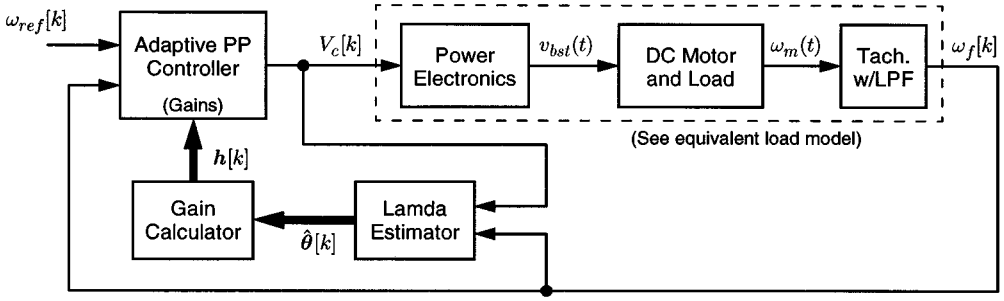

Fig. 6. Block diagram for motor speed control experiments.

the vehicle's hull to an external drive motor. Other examples might include process control or automation systems, where noncontact inductive coupling is used to transfer power across an environmental boundary. Fig. 5 illustrates the motor-speed control apparatus used for the experiments. The power electronic and data acquisition hardware is essentially identical to that described for the water bath experiment. In this case, however, the load consists of a dc motor, a variable-inertia load and a tachometer circuit. The motor was affixed securely to a support beam and used to spin a variable number of circular weights. By dropping additional weights onto the rotating shaft, the mass and hence the inertia could be changed abruptly. The shaft speed of the rotating system was sensed using a small dc motor as a tachometer. A low-pass filter circuit was used to remove brush and harmonic noise from the tachometer voltage.

A. Control Design

The multi-loop adaptive speed control system is illustrated in Fig. 6. As for the bath temperature control system, the speed controller again consists of three nested loops, where the outermost adaptive, pole placement (PP) compensated feedback loop regulates mechanical speed by controlling input voltage to the motor. This DT loops runs at a slower time scale than the inner voltage regulation loop. The remaining blocks in Fig. 6 represent the adaptive speed controller. Parameter estimation for this controller was performed using the LM-RLS algorithm.

A transfer function that relates the output filtered tachometer voltage to the input drive voltage from the boost pre-regulator can be derived with the aid of Fig. 7. The output voltage of the dc/dc stage drives a 1000 W permanent magnet dc motor. The model for this dc motor includes an armature winding resistance R_f, an armature inductance L_f and a motor back-EMF constant K_m. The motor's torque acts to rotate an inertia J against a frictional damping f. The final speed of this assembly is sensed by a small tachometer mounted to the opposite end of the motor shaft. The output voltage of the tachometer is low-pass filtered to smooth out brush noise. The transfer function of this filter is

$$\frac{\Omega_f(s)}{\Omega_m(s)} = \frac{1}{\tau_f s + 1} \tag{19}$$

where the time constant τ_f is set at approximately 10 s and $\Omega_f(s)$ and $\Omega_m(s)$ are the transforms of $\omega_f(t)$ and $\omega_m(t)$, respectively.

The motor torque can be written as

$$T_m(t) = K_m i_m = K_m \left(\frac{N_2 v_{bst}(t) - K_m \omega_m(t)}{R_d + R_f} \right) \tag{20}$$

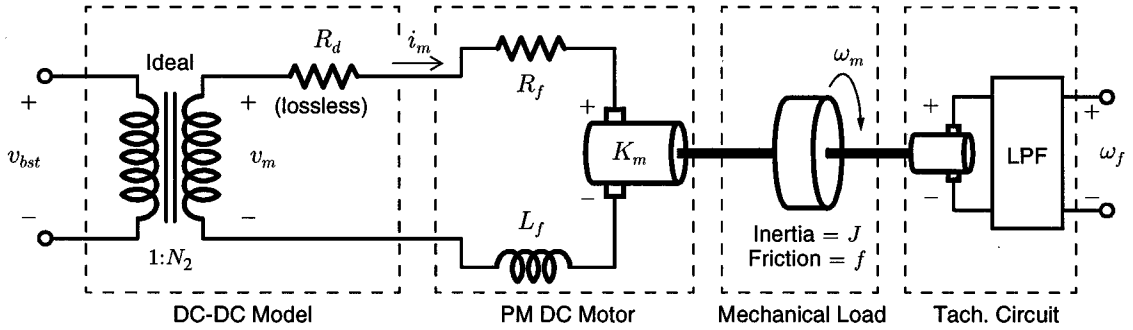

Fig. 7. Equivalent electromechanical load model.

where the effect of the winding inductance L_f has been dropped because the armature electrical time constant is considerably shorter than the sampling interval of the DT speed controller. The load torque, which balances the motor torque, is determined by the inertia, the frictional damping, and the shaft speed

$$T_L(t) = J\,\frac{d\omega_m(t)}{dt} + f\omega_m(t). \tag{21}$$

Combining (19) and the Laplace transforms of (20) and (21) yields a single CT transfer function relating the transforms of $v_{bst}(t)$ and the tachometer speed voltage $\omega_f(t)$

$$H(s) = \frac{\Omega_f(s)}{V_{bst}(s)} = \frac{g_m}{(\tau_m s+1)(\tau_f s+1)} \tag{22}$$

where

$$\tau_m = \frac{J}{f + \dfrac{{K_m}^2}{R_d+R_f}} \quad \text{and} \quad g_m = \frac{N_2 K_m}{f(R_d+R_f)+{K_m}^2}. \tag{23}$$

To complete the DT compensator design and determine the closed-loop system behavior, it is again necessary to determine the transfer function $\tilde{H}(z)$ for the dashed box in Fig. 6 that relates the z-transform of output speed to the z-transform of the input voltage command from the PP speed compensator. For the speed servo, we have exploited the time scale separation between the DT voltage and speed loops and the natural time constants of the plant to configure the voltage loop so that $\tilde{H}(z)$ can be found by applying an impulse-invariant CT-to-DT transformation [14] to the transfer function $H(s)$

$$\tilde{H}(z) = \frac{b_1 z}{z^2 + a_1 z + a_2} \tag{24}$$

where

$$\begin{aligned} b_1 &= \frac{g_m}{\tau_m - \tau_f}\left(e^{-(T_k/\tau_m)} - e^{-(T_k/\tau_f)}\right), \\ a_1 &= -\left(e^{-(T_k/\tau_m)} - e^{-(T_k/\tau_f)}\right), \\ a_2 &= e^{-((T_k/\tau_m)+(T_k/\tau_f))}. \end{aligned} \tag{25}$$

The variable T_k represents the time step of the inner voltage loop in seconds.

The impulse-invariant configuration and model for the inner voltage loop were chosen to yield an $\tilde{H}(z)$ for which a satisfactory PP compensator could be designed. This compensator provides the beneficial property of zero steady state error without requiring an explicit DT accumulator variable. Since the load is second-order, a second-order PP compensator was developed for computing the control command $V_c[k]$

$$\begin{aligned} V_c[k] = {} & d_1 V_c[k-1] + d_2 V_c[k-2] + h_1\left(\omega_{ref}[k] - \omega_f[k]\right) \\ & + \cdots h_2\left(\omega_{ref}[k] - \omega_f[k-1]\right) + h_3 \\ & \cdot \left(\omega_{ref}[k] - \omega_f[k-2]\right) \end{aligned} \tag{26}$$

where $\omega_{ref}[k]$ is the motor-speed reference command and d_1, d_2, h_1, h_2, and h_3 are constant gains. Saturation may be added in practice to limit the maximum and minimum voltage commands.

Combining (26) and the load model in (24) results in a closed-loop transfer function, which relates the transforms of the output tachometer voltage to the input command voltage, of the form

$$\tilde{H}_{CL}(z) = \frac{(1 + x_1 + x_2 + x_3 + x_4) z^3}{z^4 + x_1 z^3 + x_2 z^2 + x_3 z + x_4} \tag{27}$$

when the control gains in (26) are related to the coefficients in the closed-loop transfer function as follows:

$$\begin{aligned} d_1 &= x_4/a_2 \\ d_2 &= d_1 - 1 \\ h_1 &= (x_1 + d_1 - a_1 + 1)/b_1 \\ h_2 &= (x_2 + d_1(a_1 - 1) + a_1 - a_2)/b_1 \\ h_3 &= (x_3 + d_1(a_2 - a_1) + a_2)/b_1. \end{aligned} \tag{28}$$

Since (28) allows the coefficients of (27) to be assigned arbitrarily, the closed-loop poles may be located freely in the z-plane. One reasonable choice for a stable, well-damped response is to place the four closed loop poles at identical locations m on the real axis, i.e., $z_{1,2,3,4} = m$.

B. Adaptive Updating

Adaptive updating of the speed controller gains is accomplished using an LM-RLS parameter estimation scheme, shown in Fig. 8. The LM-RLS estimator contains at its core an RLS estimator, which is used to estimate the parameters of a low-pass

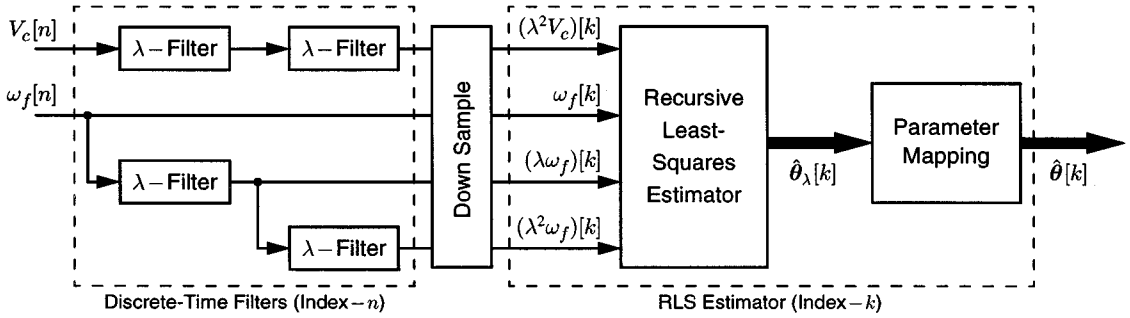

Fig. 8. Estimator.

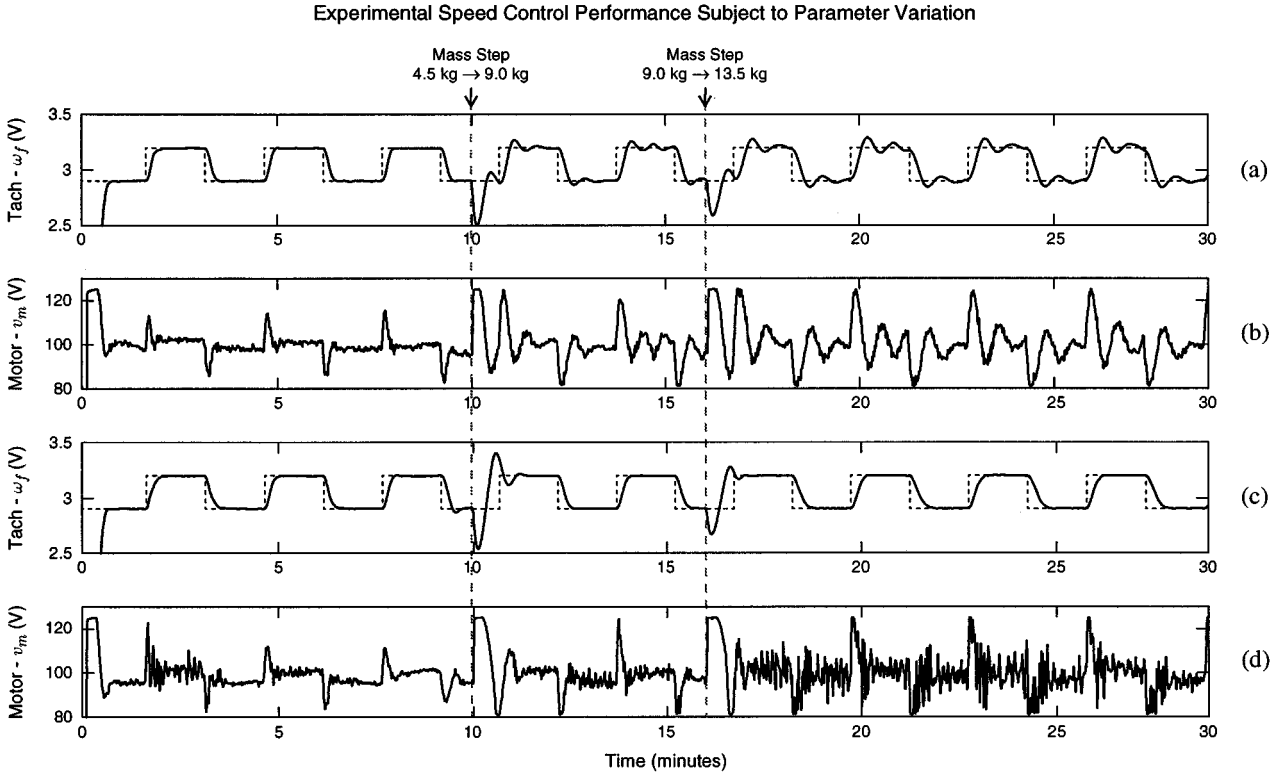

Fig. 9. Results (see text).

transformed system, and not the actual system. For this example, the regressor and the estimate vectors are, respectively

$$\mathbf{r}_\lambda[k] = \begin{bmatrix} -(\lambda\omega_f)[k] \\ -(\lambda^2\omega_f)[k] \\ (\lambda^2 V_c)[k] \end{bmatrix} \quad \text{and} \quad \hat{\boldsymbol{\theta}}_\lambda[k] = \begin{bmatrix} \hat{\alpha}_1 \\ \hat{\alpha}_2 \\ \hat{\beta}_2 \end{bmatrix}. \tag{29}$$

The operator symbol λ in (29) indicates that a particular observation is filtered. Ordinarily, a filtering operation would require that the signals are passed through an analog low-pass filter prior to being sampled. This approach is undesirable because it increases the circuit complexity. Although the filters themselves are straightforward, the number of A/D channels increases because each filtered quantity must be sampled separately. In this case four A/D channels would be required versus just two for conventional RLS.

The multirate nature of the digital control implementation provides an elegant alternative. The filtering operation can be implemented digitally at the rate of the "fast" inner voltage loop. Since the voltage-loop time index, n, steps at a rate Q times that of the outer loop, the DT filters will appear essentially continuous on the "slow" outer-loop time scale. The transfer function of each digital "λ-filter" in Fig. 8 is developed by again applying a CT-to-DT transformation to the CT transfer function of a first order low-pass filter. As shown Fig. 8, the outputs are all down-sampled to the DT time index k before entering the RLS estimator block.

The output of the RLS block is a vector $\hat{\boldsymbol{\theta}}_\lambda[k]$ of parameter estimates for the transformed load model. Estimates for the coefficients of the original CT load model in (22) can be computed according to

$$\hat{g}_m = \frac{\hat{\beta}_2}{\hat{\alpha}_1 + \hat{\alpha}_2 + 1},$$
$$\hat{\tau}_{m,f} = \frac{\tau_\lambda \hat{g}_m}{2\hat{\beta}_2}\left(2 + \hat{\alpha}_1 \pm \sqrt{\hat{\alpha}_1^2 - 4\hat{\alpha}_2}\right). \tag{30}$$

The parameter estimates that are necessary to update the speed controller can be obtained from the relationships in (25) and (28). Their application yields formulas for the quantities in $\hat{\boldsymbol{\theta}}[k]$ and $\hat{\mathbf{h}}[k]$

$$\hat{\boldsymbol{\theta}}[k] = \begin{bmatrix} \hat{a}_1 \\ \hat{a}_2 \\ \hat{b}_1 \end{bmatrix} \quad \text{and} \quad \hat{\mathbf{h}}[k] = \begin{bmatrix} \hat{d}_1 \\ \hat{d}_2 \\ \hat{h}_1 \\ \hat{h}_2 \\ \hat{h}_3 \end{bmatrix}. \tag{31}$$

The gains in $\hat{\mathbf{h}}[k]$ are used to update the coefficients of the control command, (26).

C. Results

The adaptive speed-control system was implemented in software on the 80C196KC microcontroller board. Detailed source listings can be found in [3]. Both fixed and adaptive controllers were implemented to allow for direct comparison. The fixed controller was optimized for operation with a load disk with a mass of 4.5 kg. The load model parameters for $H(s)$ in (22) were approximated experimentally at this mass setting. The results were

$$\hat{\tau}_m = 11.7 \text{ s}, \hat{\tau}_f = 10.0 \text{ s}, \text{ and } \hat{g}_m = 0.011 \text{ rads/(volt sec.)}. \tag{32}$$

The closed-loop performance of both speed-control loops was targeted to have four real poles collocated at $z = 0.70$. A sample period for the speed loop of $T_k = 1.0$ s was used, and the inner- and outer-loop DT step indices are related by $n = Qk$, where $Q = 120$. The LM-RLS parameter estimation for the adaptive controller was configured with a forgetting factor ρ of 0.97. Thus, a parameter estimate is based on approximately the last 33 s of data. Discrete time λ filters were designed to approximate CT first order filters with a time constant of 10.0 s. In our experiments, no special initial guess was supplied for $\hat{\boldsymbol{\theta}}_\lambda[k]$. Instead, the matrix $\mathbf{P}$ was initialized to 10 000 times an identity matrix, and the estimates were allowed to converge on their own. In order to assure stable control during start-up, the fixed controller was engaged for the first 1.5 min. This allowed time for the estimates to converge before adaptive control was engaged.

Experimental results are shown in Fig. 9. The top two traces in Fig. 9 show the system under the control of the fixed compensator. The top trace shows the commanded and actual tachometer voltages. The second trace shows the commanded drive voltage. The bottom two traces in the figure show the performance of the system under adaptive PP control. The third trace again shows tachometer voltage, and the fourth shows commanded drive voltage. A square wave in speed was commanded for each of the two controllers, fixed and adaptive, in order to demonstrate the control performance. The initial load mass in the experiment was set at a single disk. At this level, the closed-loop performance of both the speed controllers is nearly ideal. The step transients are consistent with the closed-loop pole locations and the tracking performance is good. The inertial mass of the system was abruptly increased at 10 min and again at 16 min into each experiment. Each increase added an additional disk to the rotating mechanical load.

The experimental results in Fig. 9 demonstrate that the adaptive controller quickly adapts to the changing inertia of the system, and that the tracking performance remains essentially constant throughout. The fixed controller fairs poorly in the face of load changes, as might be expected. The closed-loop response begins to exhibit a damped oscillatory behavior.

Each step change in the load inertia causes a definite disturbance in all three parameter estimates. In the adaptive controller, the estimates quickly converge on their new values after approximately two cycles of the step input of the system. In practice, the actual convergence time will vary depending on the excitation level of the system, the amplitude of the parameter changes, and the LM-RLS settings for ρ and τ_λ. Note that the time constant τ_λ of the "λ-filter" has an effect on the parameter convergence rate. From this perspective, an optimal setting for τ_λ is equal to or slightly smaller than the time constant associated with the fastest pole in the load model. Additional consideration must be given to provide an adequate filter for the anticipated noise environment.

VI. Discussion

The performance of the LM-RLS parameter estimation proved to be superior in a high noise environment. The motor-speed control system, for example, was subject to significant electrical noise. Noise sources included brush commutation and switching spikes. Prior to the LM-RLS experiments, an adaptive motor-speed controller was implemented using direct RLS estimation. Under nearly identical conditions, the RLS estimation proved to be erratic and unreliable. The problem was traced back in part to the covariance matrix explosion described previously. It was hoped that a judicious selection of the dead-band width δ and the forgetting factor ρ would yield satisfactory results. This was not the case. The LM-RLS method improves the situation dramatically because the regressor vector is composed of filtered measurements. Their noise content is reduced, and a much narrower dead-band δ can be tolerated.

Acknowledgment

The authors would like to thank J. Sweeney, Dr. H. Peiffer, J. Wise, Dr. J. White, Dr. G. Verghese, and Dr. B. Lesieutre for their valuable advice and support.

References

[1] G. Goodwin and K. Sin, *Adaptive Filtering Prediction and Control*. Englewood Cliffs, NJ: Prentice-Hall, 1984.
[2] R. Johansson, *System Modeling and Identification*. Engelwood Cliffs, NJ: Prentice-Hall, 1993.
[3] D. Jackson, "Inductively coupled power transfer for electromechanical systems," Ph.D. dissertation, Mass. Inst. Technol., Cambridge, May 1998.
[4] K. W. Klontz, A. Esser, P. J. Wolfs, and D. M. Divan, "Converter selection for electric vehicle charger systems with a high-frequency high-power link," in *Proc. Power Electron. Spec. Conf.*, June 1993, pp. 855–861.
[5] Society of Automotive Engineering, SAE J-1773 Electric Vehicle Inductive Coupling Recommended Practice, Warrendale, PA, Feb. 1995.

[6] A. Esser, "Contactless charging and communication system for electric vehicles," in *IEEE Ind. Applicat. Soc. Annu. Meeting*, Oct. 1993.
[7] N. Kutkut and K. Klontz, "Design considerations for power converters supplying the SAE J-1773 electric vehicle inductive coupler," in *IEEE Appl. Power Electron. Conf.*, Feb. 1997, pp. 841–847.
[8] A. W. Kelley and W. R. Owens, "Connectorless power supply for an aircraft-passenger entertainment system," *IEEE Trans. Power Electron.*, vol. 4, pp. 348–354, July 1989.
[9] A. Ghahary and B. H. Cho, "Design of a transcutaneous energy transmission system using a series resonant converter," *IEEE Trans. Power Electron.*, vol. 7, pp. 261–269, Apr. 1992.
[10] A. H. Mitwalli, S. B. Leeb, G. C. Verghese, and V. J. Thottuvelil, "An adaptive digital controller for a unity power factor converter," *IEEE Trans. Power Electron.*, vol. 11, pp. 374–382, Mar. 1996.
[11] D. Jackson, A. Schultz, S. B. Leeb, A. Mitwalli, G. Verghese, and S. R. Shaw, "A multirate digital controller for a 1.5-kW electric vehicle battery charger," *IEEE Trans. Power Electron.*, vol. 12, pp. 1000–1006, Nov. 1997.
[12] D. Jackson, S. Leeb, A. Schultz, and A. Mitwalli, "A comparison of multirate digital compensators for a battery charger," in *Proc. IEEE 5th Workshop Comput. Power Electron.*, Aug. 1996, pp. 58–65.
[13] G. H. Golub and C. F. Van Loan, *Matrix Computations*, 2nd ed. Baltimore, MD: Johns Hopkins Univ. Press, 1989, pp. 576–581.
[14] K. Astrom and B. Wittenmark, *Computer Controlled Systems*. Englewood Cliffs, NJ: Prentice-Hall, 1984.

Deron K. Jackson (M'96) received the B.S. degree in electrical engineering from the University of California, Davis, in 1991 and the M.S. and Ph.D. degrees in electrical engineering from the Massachusetts Institute of Technology, Cambridge, MA, in 1994 and 1998, respectively.

He is a Senior Hardware Engineer with Adept Technology, San Jose, CA. His research interests are in the area of power electronics and control.

Steven B. Leeb (S'89–M'93) received the B.S., M.S., E.E., and Ph.D. degrees from the Massachusetts Institute of Technology (MIT), Cambridge, in 1987, 1989, 1990, and 1993, respectively.

He has been a Member of the MIT faculty in the Department of Electrical Engineering and Computer Science since 1993. He is an Associate Professor in the Laboratory for Electromagnetic and Electronic Systems. He is concerned with the design, analysis, development, and maintenance processes for all kinds of machinery with electrical actuators, sensors, or power electronic drives.

Dr. Leeb is a Member of the IEEE Power Electronics, Control Systems, Power Engineering, and Signal Processing Societies. He is a Fellow of MIT's Leader's for Manufacturing Program and a member of Tau Beta Pi and Eta Kappa Nu.

Steven R. Shaw received the B.S. degree in electrical engineering, and the M.Eng. and Ph.D. degrees from the Massachusetts Institute of Technology (MIT), Cambridge, in 1995, 1997, and 2000, respectively.

He was a Post-Doctoral Research Assistant in the Laboratory for Electromagnetic and Electronic Systems, MIT. He is an Assistant Professor at Montana State University, Bozeman.